Extracellular processing of molecular gradients by eukaryotic cells can improve gradient detection accuracy

Igor Segota* and Carl Franck
Laboratory of Atomic and Solid State Physics, Cornell University, Ithaca 14853, USA
(Dated: September 13, 2016)

Eukaryotic cells sense molecular gradients by measuring spatial concentration differences through the difference in the number of occupied receptors to which molecules can bind. They also secrete enzymes that degrade these molecules, and it is presently not well understood how this affects the local gradient perceived by cells. Numerical and analytical results show that these enzymes can substantially increase signal-to-noise ratio of the receptor difference and allow cells to respond to a much broader range of molecular concentrations and gradients.

PACS numbers: 87.17.Jj, 82.39.Fk, 87.10.Ed, 87.10.Kn

Eukaryotic cells sense and follow molecular concentration gradients in a process called chemotaxis. This process is essential for numerous biological functions such as proliferation, organ formation, wiring of the nervous system, wound healing and cancer [1–3]. In contrast to bacteria [4], eukaryotic cells are large enough ($\gtrsim 10\,\mu$m) to be able to directly measure concentration differences across their bodies [5]. This is achieved by taking snapshots of the non-uniform occupancy of their cell surface receptors to which diffusing molecules can bind.

The physical limits of chemotactic sensitivity in eukaryotic cells have been extensively studied both theoretically and experimentally, often by calculating theoretical limits and then comparing the accuracy of the experimental chemotaxis response to these limits [5–16]. However, since many cells secrete enzymes that can inactivate chemotactic signals, the local gradient near the cell surface may differ from the gradient away from the cell.

For example, *Dictyostelium discoideum* cells secrete phosphodiesterases (PDE) [17] that inactivate cyclic adenosine monophosphate (cAMP) signals [18], *Saccharomyces cerevisiae* cells secrete Bar1 protease that degrades α-factor pheromone [19–21] and neutrophils can inactivate chemotactic formylmethionyl peptides [3]. More recently, it has been suggested that the PDE inactivation can steepen cAMP gradients in *D. discoideum* ([18], p.125) or improve the gradient direction alignment with the direction of the nearest mating partner in *S. cerevisiae* [19–21].

In *D. discoideum*, PDE exists in membrane bound and a secreted extracellular form [17, 22–24], both encoded by the same gene *pdsA*. Nanjundiah and Malchow [25] argued, using dimensional analysis, that the extracellular PDE has no observed effect. More recently, Palsson et al. [26–28] showed that within the particular parameter range of their model, PDE becomes important for wave propagation at low cell densities. Experimentally, *D. discoideum pdsA-* strain (deleted PDE gene) has been shown to fail to aggregate [29, 30] and to respond to a reduced range of cAMP concentrations compared to wild-type [31]. Despite these efforts, it remains poorly understood how exactly extracellular PDE affects the local cAMP gradient perceived by cells.

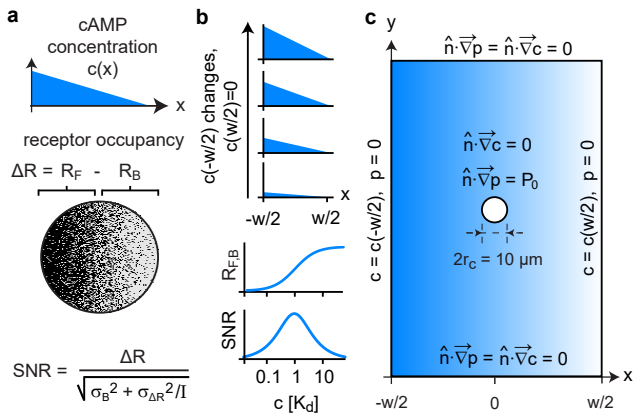

FIG. 1. Signal-to-noise ratio (SNR) and model geometry. **a**. SNR is defined as the receptor difference between the front half and back half of the cell (signal) divided by the noise consisting of receptor shot noise $\sigma_{\Delta R}$ sampled I times and non-receptor noise σ_B. **b**. When the relative gradient $|\vec{\nabla}c|/c = \text{const.}$, the optimal average concentration that maximizes SNR is $c = K_d$, since the receptor occupancy difference ΔR has maximum when $c = K_d$ and SNR $\propto \sqrt{\Delta R}$. **c**. Geometry and boundary conditions for 3D numerical simulations; c = cAMP, p = PDE concentration (not to scale). Constant relative gradient can be set away from the cell (in the bulk), by changing the cAMP concentration on the left boundary $c(-w/2)$, while keeping $c(w/2) = 0$. $w = 1\,$mm.

We address this question by calculating cAMP concentration around the cell using 3D reaction-diffusion models of cAMP-PDE interaction in the extracellular space, for a typical microfluidic geometry [16, 32] and in space where a cell is detecting cAMP emitted by a point source. We use these results to calculate the gradient detection signal-to-noise ratio (SNR) of the receptor response following Rappel and Levine [9] and van Haastert and Postma [33] and predict how the chemotaxis index is affected by extracellular PDE.

We can gain some intuition about SNR by considering a linearly increasing cAMP concentration $c(x)$ in 1D. Assuming the steady state of cAMP to cAMP-receptor binding, each receptor at coordinate x can be thought of as a Bernoulli trial with the probability of being occupied $p(x) = c(x)/[c(x) + K_d]$ and unoccupied with probability $1 - p(x)$, where K_d is the cAMP to cAMP-receptor binding dissociation constant (SI, Section 1). Since the receptor distribution on the cell surface is uniform [34] and cAMP concentration $c(x) = c_0 - |\vec{\nabla}c|x$, we can consider having half receptors on each cell half at $x = \mp r_c/2$ (r_c is cell radius, cell is centered at $x = 0$). The distribution of the number of occupied receptors on each half of the cell follows a Binomial distribution with the average and variance:

$$R_{F,B} = \frac{N}{2}\frac{c_{F,B}}{c_{F,B} + K_d}, \quad \sigma^2_{R_{F,B}} = \frac{N}{2}\frac{c_{F,B}K_d}{(c_{F,B} + K_d)^2} \quad (1)$$

where $c_{F,B} = c(\mp r_c/2)$ and N is the total number of receptors per cell; here $K_d = 30\,\mathrm{nM}$, $N = 70,000$ [35]. SNR is defined as [9, 33] (Fig.1a):

$$\mathrm{SNR} = \frac{\Delta R}{\sqrt{\sigma^2_B + \sigma^2_{\Delta R}/I}}, \Delta R = R_F - R_B \quad (2)$$

where ΔR and $\sigma^2_{\Delta R} = \sigma^2_{R_F} + \sigma^2_{R_B}$ are the average ("signal") and variance (square of the "noise") of the difference of occupied receptors at the front and back half of the cell, σ_B the non-receptor noise and I is the the number of statistically independent measurements of the occupied receptors [33].

For shallow gradients, the concentration difference between the cell front and back is small ($r_c|\vec{\nabla}c| \ll K_d$) so the average and variance of the receptor difference are (SI, Section 2):

$$\Delta R \approx \frac{N}{2}\frac{K_d r_c|\vec{\nabla}c|}{(c_0 + K_d)^2}, \quad \sigma^2_{\Delta R} \approx N\frac{c_0 K_d}{(c_0 + K_d)^2} \quad (3)$$

For fixed relative gradients $|\vec{\nabla}c|/c_0 = \text{const.}$: (i) the receptor occupancy $R_{F,B}$ has the steepest increase at $c_0 = K_d$, so $\Delta R \propto dR/dc$ is maximal, and (ii) the receptor noise is proportional to the square root of the signal $\sigma_{\Delta R} \propto \sqrt{\Delta R}$. Then, SNR is also proportional to the square root of the signal: $\mathrm{SNR} \propto \Delta R/\sqrt{\Delta R} = \sqrt{\Delta R}$ and also maximal at $c_0 = K_d$ (Fig.1b). Therefore, the optimal average cAMP concentration for gradient sensing without PDE is at exactly K_d when the receptor occupancies are $\approx 50\%$.

For parameter values $\sigma_B = 73$ and $I = 1.4$ the measured chemotaxis index (CI) was fit to the empirical equation $\mathrm{CI} = \mathrm{SNR}/(\mathrm{SNR} + 1)$; see SI Section 3.

Fixed PDE secretion flux model.— We consider a system of two interacting molecules, PDE and cAMP, following Michaelis-Menten kinetics:

$$\mathrm{PDE} + \mathrm{cAMP} \underset{k_{-1}}{\overset{k_1}{\rightleftharpoons}} C_{cp} \xrightarrow{k_2} \mathrm{PDE} + 5'\mathrm{AMP} \quad (4)$$

where k_i represent the reaction rates, C_{cp} represents the intermediate cAMP-PDE complex and 5'AMP the product of this reaction (a deactivated signal).

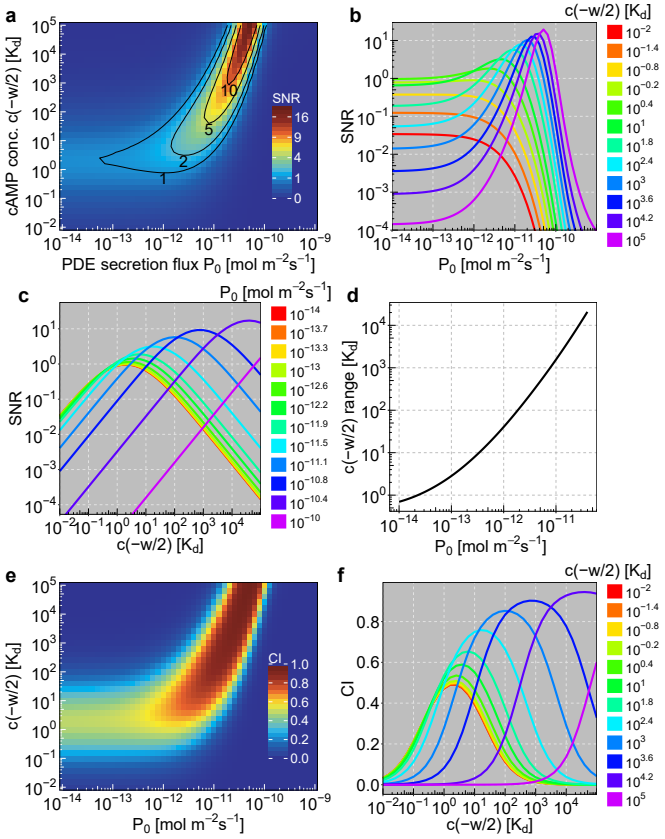

FIG. 2. Fixed PDE secretion flux model with relative gradient on the cell body is 1%. **a**. SNR as a function of PDE secretion flux P_0 and cAMP boundary concentration $c(-w/2)$. SNR can be substantially improved by PDE for a range of parameters P_0 and $c(-w/2)$. **b**. Horizontal slices from a. PDE can increase SNR for $c(-w/2) \gtrsim K_d$. **c**. Vertical slices from a. Increasing P_0 shifts the optimal cAMP concentration (maximizing SNR) towards higher values but also broadens the detectable range of cAMP concentrations. The red curve for $P_0 = 10^{-14}\,\mathrm{mol\,m^{-2}s^{-1}} \approx 0$, i.e. matches SNR in Fig.1b. **d**. Broadening of curves from c is quantified by calculating the range of $c(-w/2)$ for which SNR ≥ 1. **e**. Chemotaxis index (CI) calculated as SNR/(SNR + 1) (SI Section 3). **f**. Vertical slices from e.

The concentrations of cAMP $c(\vec{r}, t)$, PDE $p(\vec{r}, t)$, cAMP-PDE complex $C_{cp}(\vec{r}, t)$ and the 5'AMP $c'(\vec{r}, t)$, are obtained in the standard quasi-steady state assumption [36] (intermediate complex is in steady state): $k_1 cp = (k_{-1} + k_2)C_{cp}$, so the two relevant steady-state equations are (SI, Section 4):

$$D_c\nabla^2 c - \frac{k_2}{K_M}pc = 0, \quad D_p\nabla^2 p = 0 \quad (5)$$

where D_c and D_p are the diffusion constants of cAMP and PDE and $K_M \equiv (k_{-1} + k_2)/k_1$. These equations

are solved numerically using COMSOL 3.5 (Comsol Inc.) with MATLAB R2011a (The MathWorks, Inc.) for the boundary conditions mimicking typical experiments [16, 37, 38], (Fig.1c and SI Section 5). cAMP concentration is varied on the left boundary $c(x{=}-w/2)$, zero on the right boundary $c(x{=}w/2) = 0$ and the normal component of cAMP flux is zero everywhere else, including the cell boundary [39]. These boundary conditions result in constant applied relative gradient $|\vec{\nabla}c|_{\rm app}/c_{0,\rm app}$, where $|\vec{\nabla}c|_{\rm app} = [c(-w/2) - c(w/2)]/w = c(-w/2)/w$ and $c_{0,\rm app} = [c(-w/2) + c(w/2)]/2 = c(-w/2)/2$. For PDE concentration, $p(x{=}\pm w/2) = 0$ and its normal flux is zero everywhere except for the cell boundary where it is P_0. The parameters used in simulations were: $K_M = 10\,\mu$M [40], $D_c = 444\,\mu\mathrm{m}^2\mathrm{s}^{-1}$ [41], $D_p = 70\,\mu\mathrm{m}^2\mathrm{s}^{-1}$, $k_2 = 13,300\,\mathrm{s}^{-1}$(estimated; SI, Section 6), $r_c = 5\,\mu$m.

Fig.2a shows SNR, as a function of PDE secretion flux P_0 and cAMP concentration on the left boundary $c(-w/2)$, for the relative gradient $r_c|\vec{\nabla}c|_{\rm app}/c_{0,\rm app} = 2r_c/w = 1\%$ across the cell body. PDE can substantially improve SNR for a range of P_0 and $c(-w/2)$ values and the improvement is better for large cAMP concentrations. If the midpoint concentration is $\lesssim K_d$ ($c(-w/2) \lesssim 2\,K_d$), then SNR can only be decreased by PDE (Fig.2b). PDE can also broaden the range of cAMP detection by increasing the $c(-w/2)$ range for which SNR ≥ 1 (Fig.2c,d). This behavior is also reflected in the CI (Fig.2e,f). The SNR improvement by PDE also occurs when either the absolute gradient $|\vec{\nabla}c|_{\rm app}$ or the midpoint concentration $c_{0,\rm app}$ are fixed (SI, Section 7).

According to Fig.2, the relevant P_0 range between 10^{-12} and $10^{-10}\,\mathrm{mol\,m^{-2}s^{-1}}$, falls within the rough physiological range estimated here for PDE of $10^{-11}\,\mathrm{mol\,m^{-2}s^{-1}}$ (SI Section 6.3) and by others for Bar1 of $10^{-12}\,\mathrm{mol\,m^{-2}s^{-1}}$ (which degrades α-factor pheromone signal in yeast) [20].

Next, we analyze how the increase in SNR is achieved. PDE reduces the gradient but even more the average concentration across the cell body (Fig.3a), so the signal $\Delta R \propto |\vec{\nabla}c|/(c_0 + K_d)^2$ is enhanced (Fig.3b). For $P_0 \lesssim 10^{-10}\,\mathrm{nM}\,\mu\mathrm{m}^{-1}$, PDE can generate up to ~ 1000 receptors difference. On the other had, the noise has both an upper bound of $\sqrt{\sigma_B^2 + N/(4I)} \approx 134$ at $c_0 = K_d$ (Eq.3) and a lower bound due to the non-receptor noise $\sigma_B = 73$ (Fig.3c). Both bounds follow directly from the definition, Eqs.2,1 and imply that the overall scale of the noise is largely PDE-independent. This results in the SNR enhancement that comes directly from the signal increase, which can be more than an order of magnitude for $c_0 \gtrsim 100\,K_d$ (Fig.3d).

Fixed PDE concentration models.— We consider two models with spatially uniform PDE concentration $p(\vec{r}, t) = p_0$. For the case with same microfluidic geometry as before but without cell boundary in the middle,

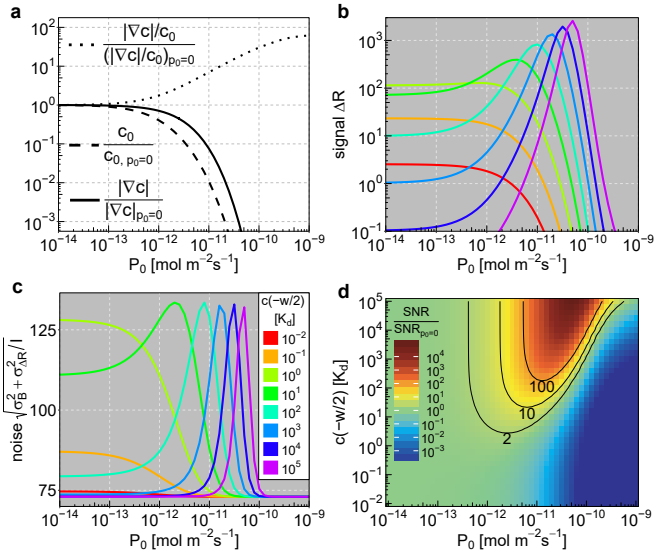

FIG. 3. Signal and noise analysis of the Fixed PDE secretion flux model. **a**. Mean cAMP concentration c_0 and gradient $|\vec{\nabla}c|$ across the cell surface, as a function of PDE secretion flux P_0. **b**. Signal $\Delta R(P_0) \propto |\vec{\nabla}c|/(c_0 + K_d)^2$. Color legend is the same as in c. **c**. Noise $\sqrt{\sigma_B^2 + \sigma_{\Delta R}^2/I}$, with lower limit $\sigma_B = 73$ and upper limit $\sqrt{\sigma_B^2 + N/(4I)} \approx 134$. **d**. Ratio of SNR and SNR with $P_0 = 0$. Most of the SNR enhancement results from the enhancement of the signal ΔR.

the exact analytical solution of Eq.5 is:

$$c(x) = c(-w/2)\frac{\sinh\left(\frac{w}{2L} - \frac{x}{L}\right)}{\sinh\left(\frac{w}{L}\right)}, \quad L = \sqrt{\frac{K_M D_c}{k_2 p_0}} \qquad (6)$$

where now a degradation length L appears in the gradient sensed by the cell. At $x = 0$, the cAMP concentration and gradient are:

$$|\vec{\nabla}c| = \frac{c(-w/2)}{2L\sinh\left(\frac{w}{2L}\right)}, \quad c_0 = \frac{c(-w/2)}{2\cosh\left(\frac{w}{2L}\right)} \qquad (7)$$

The analytical expression for SNR can be simplified under the approximation of shallow gradients $r_c|\vec{\nabla}c| \ll K_d$ which is well satisfied in this work ($\max(r_c|\vec{\nabla}c|/K_d) = 5 \cdot 10^{-3}$):

$$\mathrm{SNR} \approx \frac{N K_d r_c |\vec{\nabla}c|}{2(c_0 + K_d)\sqrt{\sigma_B^2(c_0 + K_d)^2 + N c_0 K_d}} \qquad (8)$$

This SNR is calculated using Eqs.7 (Fig.4a,b) and shows very similar behavior to the Fixed PDE secretion flux model. Intuitively, PDE converts the original relative gradient $\propto r_c/w$ to a new one $\propto r_c/L$ for $L \ll w$ (SI, Section 8.1). The presence of a cell boundary to a large extent only changes the overall scaling factor (SI, Section 8.2).

Finally, we consider the case of cAMP emitted by the point source in full 3D space. Without PDE, the solu-

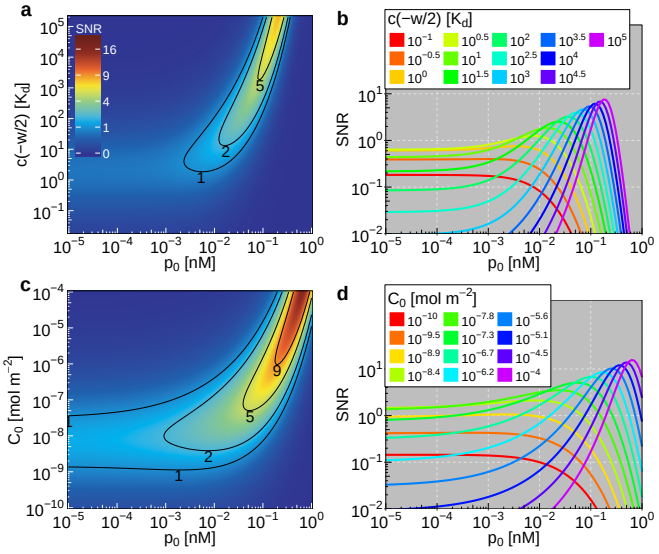

FIG. 4. Analytical exact solutions for SNR for Fixed PDE concentration models. **a,b**. Microfluidic geometry: SNR as a function of PDE concentration p_0 and cAMP concentration on the left boundary $c(-w/2)$. **c,d**. cAMP point source $C_0\delta(r)$ located at $\vec{r}=0$: SNR as a function of cAMP source strength C_0 and p_0 at a distance $r = 225\,\mu$m from the source.

tion of the steady-state diffusion equation for cAMP concentration $c(\vec{r})$ is equivalent to the electrostatic potential from the point charge located at origin, $c(\vec{r}) \sim 1/r$. With uniform PDE, the cAMP concentration becomes $c(r) = C_0 e^{-r/L}/r$ (SI, Section 8.3) and is equivalent to ion screening in classical plasma [42], with L having the role of Debye length. We again observe same effect on SNR at distances below $\sim 0.5\,$mm from the source (Fig.4c,d, SI Fig.8).

Concluding remarks.— In summary, we investigated the effects of extracellular PDE on cAMP gradient sensing in *D. discoideum*. We find that PDE secretion by cells shifts their response towards higher cAMP concentrations (as expected) but can also greatly increase the SNR and broaden the range of signal detection. This contrasts an earlier conclusion reached using dimensional analysis [25]. The SNR increase is directly related to the increase in the signal (differential receptor occupancy), while the noise has a PDE-independent upper bound.

Our model results qualitatively agree with (i) previous observations of *pdsA*- cells responding to a narrower range of cAMP concentrations [31] and (ii) decrease in CI if the cells are starved for longer time periods, and exposed to the same gradient (Fig.4 in [38]) since the peak response would shift towards higher cAMP concentrations if the PDE accumulates in the environment. CI could also measured for the range of cAMP concentrations for both wild-type and *pdsA*- cells and compared to the predictions of our model.

The effects discussed here also lead to different predictions between the experiments with static non-flowing gradients where cAMP gradients are affected by secreted PDE [16, 37, 38] and the experiments with static gradients establish with flow [11, 13, 14]. The flow gradient experiments are considered advantageous since the cells are prevented to communicate with each other with cAMP (while not significantly distorting the local gradient around the cell [43]), however they also completely wash away extracellular PDE (SI, Section 9).

Finally, we neglected the effects of PDE inhibitor, which is expected to get secreted under high PDE levels [44] and would effectively increase the Michaelis-Menten constant of the cAMP-PDE interaction K_M towards millimolar range [40].

ACKNOWLEDGMENTS

We thank Cornell ACCEL computer lab for the access to COMSOL Multiphysics and MATLAB software, and anonymous referees for insightful suggestions.

* Present address: Department of Physics, University of California San Diego; is246@cornell.edu

[1] K. Swaney, C. Huang, and P. Devreotes, Annu. Rev. Biophys. **39**, 265 (2010).
[2] E. Roussos, J. Condeelis, and A. Patsialou, Nat. Rev. Cancer **11**, 573 (2011).
[3] S. Zigmond, J. Cell. Biol. **75**, 606 (1977).
[4] V. Sourjik and N. Wingreen, Curr. Opin. Cell Biol. **24**, 262 (2012).
[5] H. Berg and E. Purcell, Biophys. J. **20**, 193 (1977).
[6] R. Endres and N. Wingreen, Proc. Natl. Acad. Sci. USA **105**, 15749 (2008).
[7] T. Mora and N. Wingreen, Phys. Rev. Lett. **104**, 248101 (2010).
[8] B. Hu, W. Chen, J.-W. Rappel, and H. Levine, Phys. Rev. Lett. **105**, 048104 (2010).
[9] J.-W. Rappel and H. Levine, Proc. Natl. Acad. Sci. USA **105**, 19270 (2008).
[10] B. Hu, W. Chen, H. Levine, and J.-W. Rappel, J. Stat. Phys. **142**, 1167 (2011).
[11] D. Fuller, W. Chen, M. Adler, A. Groisman, H. Levine, J.-W. Rappel, and W. Loomis, Proc. Natl. Acad. Sci. USA **107**, 9656 (2010).
[12] M. Ueda and T. Shibata, Biophys. J. **93**, 11 (2007).
[13] L. Song, S. Nadkarni, H. Bodeker, C. Beta, A. Bae, C. Franck, J.-W. Rappel, W. Loomis, and E. Bodenschatz, Eur. J. Cell Biol. **85**, 981 (2006).
[14] G. Amselem, M. Theves, A. Bae, C. Beta, and E.Bodenschatz, Phys. Rev. Lett. **109**, 108103 (2012).
[15] G. Amselem, M. Theves, A. Bae, E. Bodenschatz, and C. Beta, PLoS ONE , 7(5):e37213 (2012).
[16] I. Segota, S. Mong, E. Neidich, A. Rachakonda, C. J. Lussenhop, and C. Franck, J. R. Soc. Interface **10**, 20130606 (2013).
[17] Y. Chang, Science **161**, 57 (1968).

[18] R. Kessin, *Dictyostelium: Evolution, Cell Biology and the Development of Multicellularity* (Cambridge University Press, 2001).

[19] N. Barkai, M. Rose, and N. Wingreen, Nature **396**, 422 (1998).

[20] S. Andrews, N. Addy, R. Brent, and A. Arkin, PLoS Comp. Biol. , 6:e1000705 (2010).

[21] M. Jin, B. Errede, M. Behar, W. Mather, S. Nayak, J. Hasty, H. Dohlman, and T. Elston, Sci. Signal. **4**, ra52 (2011).

[22] R. Shapiro, J. Franke, E. Luna, and R. Kessin, Biochim. Biophys. Acta **758**, 49 (1983).

[23] S. Bader, A. Kortholt, and P. van Haastert, Biochem. J. **402**, 153 (2007).

[24] S. Orlow, R. Shapiro, J. Franke, and R. Kessin, J. Biol. Chem. **256**, 7620 (1981).

[25] V. Nanjundiah and D. Malchow, J. Cell Sci. **22**, 49 (1976).

[26] E. Palsson and E. Cox, Proc. Natl. Acad. Sci. USA **93**, 1151 (1996).

[27] E. Palsson, K. Lee, R. Goldstein, J. Franke, R. Kessin, and E. Cox, Proc. Natl. Acad. Sci. USA **94**, 13719 (1997).

[28] E. Palsson, Biophys. J. **97**, 2388 (2009).

[29] J. Barra, P. Barrand, M. Blondelet, and P. Brachet, Mol. Gen. Genet. **177**, 607 (1980).

[30] R. Sucgang, C. Weijer, F. Siegert, J. Franke, and R. Kessin, Dev. Biol. **192**, 181 (1997).

[31] G. Garcia, E. Rericha, C. Heger, P. Goldsmith, and C. Parent, Mol. Biol. Cell **20**, 3295 (2009).

[32] S.-Y. Cheng, S. Heilman, M. Wasserman, S. Archer, M. Shulerac, and M. Wu, Lab Chip **7**, 763 (2007).

[33] P. van Haastert and M. Postma, Biophys. J. **93**, 1787 (2007).

[34] T. Jin, N. Zhang, Y. Long, C. Parent, and P. Devreotes, Science **287**, 1034 (2000).

[35] R. Johnson, P. van Haastert, A. Kimmel, C. S. III, B. Jastorff, and P. Devreotes, J. Biol. Chem. **267**, 4600 (1992).

[36] J. Borghans, R. D. Boer, and L. Segel, Bull. of Math. Biology **58**, 43 (1996).

[37] B. Varnum and D. Soll, J. Cell Biol. **99**, 1151 (1948).

[38] P. Fisher, R. Merkl, and G. Gerisch, J. Cell. Biol. **108**, 973 (1989).

[39] Zero-normal cAMP flux seems reasonable since the time scale for receptor internalization is 5 minutes [A. Serge et al. Integr. Biol., 3, 675-683, 2011] compared to the time scale of receptor dissociation of 1 second [M. Ueda et al. Science, 294, 864-867, 2001], so the binding and unbinding processes are in equilibrium.

[40] R. Kessin, S. Orlow, R. Shapiro, and J. Franke, Proc. Natl. Acad. Sci. USA **76**, 5450 (1979).

[41] M. Dworkin and K. H. Keller, J. Biol. Chem. **252**, 864 (1977).

[42] L. Landau and E. Lifshitz, *Statistical Physics, 3rd Ed.* (Pergamon Press, 1996) p. 241.

[43] C. Beta, T. Frohlich, H. Bodeker, and E. Bodenschatz, Lab Chip **8**, 1087 (2008).

[44] J. Franke and R. Kessin, J. Biol. Chem. **256**, 7628 (1981).